Momentum-resolved conductivity of strongly interacting bosons in an optical lattice

B. Grygiel and T. A. Zaleski

Institute of Low Temperature and Structure Research, Polish Academy of Sciences, Okólna 2, 50-422 Wrocław, Poland

Motivated by the recent advancements in experimental techniques in the cold atomic systems, we study the dependence of the conductivity on momentum in a system of strongly interacting bosons in an optical lattice. By employing the quantum rotor approach to the Bose-Hubbard model we calculate the current-current correlation function and subsequently obtain the analytic formula for the momentum-dependent longitudinal conductivity. We analyze the behavior of the conductivity for the square and cubic lattices in both, the superfluid and Mott insulator phases. As a consequence of the particle-hole symmetry, the conductivity for a uniformly filled lattice in the superfluid phase exhibits a linear dependence for a surprisingly wide range of momenta around $\mathbf{k} = 0$. This allows us to predict the value of the group velocity of the particle excitations. We also consider the impact of finite temperature and discover that it leads to an additional conductivity channel, which is aligned along the direction of the probe field and located within the energy gap.

I. INTRODUCTION

In recent years ultracold atomic systems have become very popular and intensely studied. Owing to their high controllability and lack of nonintentional defects they can serve as versatile platforms for quantum simulations of solid-state systems [1–4]. Lately, a lot of effort has been made to propose and develop experimental setups which allow the study of transport phenomena of ultracold atoms [5–7]. The most prominent transport measurements were conducted at ETH Zürich. A series of experiments with the flow of atoms between two reservoirs with a narrow constriction between them allowed for verification of quantized conductance in accordance with the Landauer theory [8,9]. This setup, which can be thought of as a cold atomic equivalent of a quantum point contact device, was also used to study the effects of temperature, disorder, dissipation, and interaction on particle transport [10–13] as well as spin-splitting effects [14]. Another new technique is scanning probe microscopy. It is analogous to scanning gate microscopy in semiconducting systems and allows for obtaining high-resolution maps of transport in cold atomic systems [15]. A single-site-resolved measurement protocol has also been proposed, which could provide a way to measure the current statistics of the interacting bosons in an optical lattice [16].

Another way to investigate the transport properties of the system is to study the current-current correlation function, which is directly proportional to the conductivity. In 2011 Tokuno and Giamarchi [5] proposed an experimental setup in which the current-current correlation function could be obtained from the energy absorption rate in a periodically modulated optical lattice. This idea was further developed by Wu *et al.* [6] to extract the conductivity as a linear response of the gas in an optical lattice to a time-dependent displacement of the harmonic trapping potential. This can be

thought of as an analog of an external electric field acting on a condensed-matter system. Recently, this proposal was experimentally realized in a fermionic optical lattice [17].

The transport properties of strongly correlated lattice systems have also been studied theoretically in many contexts, e.g., in Josephson junction arrays [18–20], superconductors [21], granular superconductors [22], one-dimensional, dissipative bosonic systems [23–26], and optical lattices with ultracold bosonic gases [27–31]. However, the optical lattice system provides the best and most direct comparison between the theoretical predictions and experimental results. Thus, it is our goal to analyze the momentum-resolved conductivity of strongly interacting bosons in a lattice. We derive the momentum-resolved conductivity as a response function of the system to a small, spatially nonuniform electric field. In order to obtain the spatial current-current correlation functions, which are directly related to the conductivity, we rely on the quantum rotor approach (QRA) applied to the Bose-Hubbard (BH) model [32]. A great advantage of this approach is that it takes into account the spatial fluctuations; thus, it is especially useful to describe systems in spatially dependent gauge potentials and analyze direction-dependent observables, which is crucial to accomplish our goal [31,33].

The remainder of this paper is organized in the following way. In Sec. II, we briefly present the quantum rotor approach applied to the Bose-Hubbard model. Section III is devoted to the derivation of the momentum-resolved conductivity and the analysis of its behavior in the ground state (Sec. III A) and at finite temperatures (Sec. III C). The details of the calculation are relegated to the Appendix. The paper is summarized in Sec. IV.

II. BOSE-HUBBARD MODEL IN THE QUANTUM ROTOR APPROACH

A. Hamiltonian

In order to describe the system of strongly interacting bosons in an optical lattice we employ the Bose-Hubbard

*Corresponding author: b.grygiel@intibs.pl

model [34,35]:

$$\hat{H} = -t \sum_{\langle l,l' \rangle} \left[\exp\left(\frac{2\pi i}{\Phi_0} \int_{\mathbf{r}_{l'}}^{\mathbf{r}_l} \mathbf{A}(\mathbf{r}, t) \cdot d\mathbf{s} \right) \hat{a}_l^{\dagger} \hat{a}_{l'} + \text{H.c.} \right]$$
$$+ \frac{U}{2} \sum_l \hat{n}_l(\hat{n}_l - 1) - \mu \sum_l \hat{n}_l. \quad (1)$$

In the standard notation, t is the bare tunneling coefficient of the atoms between the neighboring sites, U is the energy of the on-site repulsive interaction, and μ is the chemical potential. The symbol $\langle l, l' \rangle$ refers to the set of pairs of neighboring lattice sites, with l defined as a vector of the position coordinates (l_x, l_y, l_z). The operators $\hat{a}_l^{\dagger}$ and $\hat{a}_l$ denote the processes of creation and annihilation of bosons, respectively, and the operator $\hat{n}_l$ is the number operator on the lth lattice site.

To account for the presence of the external electric field, the hopping term includes a phase factor dependent on the vector potential $\mathbf{A}(\mathbf{r}, t)$, which is known as the Peierls substitution [36]. The quantity Φ_0 denotes the flux quantum, and the integral is calculated along the trajectory of a particle tunneling between neighboring lattice sites.

B. Longitudinal conductivity

In the present paper, we restrict our considerations to the longitudinal conductivity. The transverse response vanishes for the considered square and cubic lattice systems when the external gauge potentials (except for the probe electric field) are not present [19]. It should be noted that arbitrary gauge potentials leading to a "synthetic" magnetic field can be realized in optical lattices [37] and can also be described within the framework of the quantum rotor approach on which we are relying; however, they are not considered in the present paper.

To obtain the conductivity in the linear response regime, we first represent the partition function of the Bose-Hubbard system as a path integral in Matsubara "imaginary time" $0 \leqslant \tau \leqslant \beta = 1/k_B T$, where k_B denotes the Boltzmann constant and T is the temperature. With the help of the coherent state representation we are able to rewrite the BH Hamiltonian (1) in terms of the complex bosonic fields $\bar{a}_l(\tau)$ and $a_l(\tau)$ instead of the creation and annihilation operators while keeping its original form [38].

The partition function of the system is given as

$$Z = \int [\mathcal{D}\bar{a} \, \mathcal{D}a] \, e^{-S[\bar{a},a]}, \quad (2)$$

where the action consists of two terms:

$$S[\bar{a}, a] = \int_0^{\beta} d\tau \left(H[\bar{a}, a] + \sum_l \bar{a}_l(\tau) \frac{\partial a_l(\tau)}{\partial \tau} \right). \quad (3)$$

The first term includes the Hamiltonian (1) of the system in the coherent state representation, while the second term is the so-called Berry term, which appears because the system acquires a geometric phase during the evolution from time $\tau = 0$ to $\tau = \beta$. For simplicity of the notation, we assume that $\hbar = 1$.

Within the linear response theory [39] the momentum-resolved conductivity $\sigma_{ij}(\mathbf{k}, \omega_\nu)$ is defined as a response of the system to an infinitesimally small external electric field,

here represented by its vector potential $\mathbf{A}(\mathbf{r}, \tau)$:

$$\sigma_{ij}(\mathbf{k}, \omega_\nu) = -\frac{1}{N\beta\omega_\nu} \sum_{l,l'} \int_0^{\beta} d\tau \, d\tau'$$
$$\times \left. \frac{\delta^2 \ln Z}{\delta A_j(\mathbf{r}_{l'}, \tau') \, \delta A_i(\mathbf{r}_l, \tau)} \right|_{\mathbf{A}=0}$$
$$\times e^{i[\mathbf{k}(\mathbf{r}_l - \mathbf{r}_{l'}) - \omega_\nu(\tau - \tau')]}, \quad (4)$$

where indices $i, j = x, y, z$ refer to the direction in space and $\omega_\nu = 2\pi\nu/\beta$ ($\nu = 0, \pm 1, \pm 2, \dots$) is the bosonic Matsubara frequency.

Substituting the partition function (2) in formula (4) and performing the second-order functional derivative yield the longitudinal conductivity in the x direction in the following form:

$$\sigma_{xx}(\mathbf{k}, \omega_\nu) = \frac{1}{(N\beta)^3 \omega_\nu} \left\{ \frac{4\pi^2 t^2}{\Phi_0^2} \sum_{\mathbf{q},m} [\sin(q_x) + \sin(q_x + k_x)]^2 \right.$$
$$\times \langle \bar{a}_{\mathbf{q}+\mathbf{k},m+\nu} a_{\mathbf{q}+\mathbf{k},m+\nu} \rangle \langle \bar{a}_{\mathbf{q},m} a_{\mathbf{q},m} \rangle$$
$$+ \frac{8\pi^2 t}{\Phi_0^2} \sum_{\mathbf{q},m} [\sin^2(q_x) + \sin(q_x)\sin(q_x + k_x)]$$
$$\left. \times \langle \bar{a}_{\mathbf{q},m} a_{\mathbf{q},m} \rangle^2 \right\}, \quad (5)$$

where we have restricted our considerations to the systems defined on the simple square and cubic lattices (although the method can be generalized to other lattices). A detailed derivation of formula (5) is presented in the Appendix.

C. Quantum rotor approach

In order to obtain the current-current correlation function of the BH model, we employ the quantum rotor approach [32]. This technique is based on earlier methods of slave rotors [40,41] and quantum rotors developed for fermionic systems [42] (for differences in these approaches, see Ref. [43]). The QRA relies on a basis change from the particle-number representation to the conjugate phase representation of the bosonic fields. This is especially useful for studying the superfluid (SF)–Mott insulator (MI) phase transition, which is driven by the quantum phase fluctuations. As a result, the system of strongly interacting bosons in a lattice is transformed to an effective phase model of interacting quantum rotors [32]. The QRA allows us to take into account the spatial fluctuations and thus to capture the influence of the lattice geometry and external gauge potentials on the phase diagram of the SF-MI transition and other properties of the system. Moreover, it is consistent with Mermin-Wagner theorem; that is, it properly captures the phase transitions in two-dimensional (2D) systems at zero temperature and in three-dimensional (3D) systems at finite temperatures [44]. Also, its predictions are comparable with the quantum Monte Carlo results [32]. The QRA was successfully applied to describe quantum phase transitions [45]; magnetic and superconducting systems [42,46,47], including systems of Josephson junction arrays [48]; and phase

transition in spin glasses [49] and in ultracold atomic systems in optical lattices [31–33,50–52].

The crucial step in the quantum rotor approach is the gauge transformation of the complex fields $\bar{a}_l(\tau)$ and $a_l(\tau)$. More precisely, it is a rotation in the complex plane with the $\phi_l(\tau)$ phase:

$$a_l(\tau) = b_l(\tau)e^{i\phi_l(\tau)},$$
$$\bar{a}_l(\tau) = \bar{b}_l(\tau)e^{-i\phi_l(\tau)}. \qquad (6)$$

This transformation allows us to express the variables by the amplitude $b_l(\tau)$ and phase $\phi_l(\tau)$ degrees of freedom. The former is related to the superfluid density, while the latter is related to the phase of the condensate.

The superfluid order parameter Ψ_{SF} can now be factorized:

$$\Psi_{SF} = \langle a_l(\tau) \rangle = \langle b_l(\tau) \rangle \langle e^{i\phi_l(\tau)} \rangle, \qquad (7)$$

which indicates that not only is a nonzero amplitude of the condensate required for the system to be in the ordered phase but also the system must exhibit a long-range phase coherence, $\langle e^{i\phi_l(\tau)} \rangle \neq 0$, related to the spontaneous U(1) symmetry breaking.

As the SF-MI phase transition is driven by the phase fluctuations, the amplitude fluctuations can be neglected to simplify the calculations [22]. This allows us to take the value of the on-site amplitude as an average, $b_l(\tau) = \langle b_l(\tau) \rangle + \delta b_l(\tau) \approx \langle b_l(\tau) \rangle = b_0$, with

$$b_0 = \sqrt{\frac{t(tz + \bar{\mu})}{U}}, \qquad (8)$$

where z is the number of nearest neighbors and $\bar{\mu} = \mu + U/2$ is the shifted chemical potential. This approach is justified because at low temperatures the considered system is uniform. Equation (8) naturally dictates the range of the validity of the QRA. The approach works well for the finite values of the ratio t/U, which corresponds to the average and strong coupling limits.

Nonetheless, the amplitude fluctuations can also be included in the QRA via the Bogoliubov method. This enables the study of the spectral functions and momentum distribution of the atoms, which exhibit very good agreement with the results of time-of-flight experiments [50,51].

The gauge transformation (6) allows us to express the partition function of the system only in terms of the phase variables $\phi_l(\tau)$ by means of the cumulant series expansion [32]

$$Z = \int [\mathcal{D}\phi] e^{-S[\phi]}, \qquad (9)$$

where the action $S[\phi]$ is the action of the interacting quantum rotors:

$$S[\phi] = \int_0^\beta d\tau \left\{ -2J \sum_{\langle l,l' \rangle} \cos[\phi_l(\tau) - \phi_{l'}(\tau)] \right.$$
$$\left. + \sum_l \left[\frac{\dot{\phi}_l^2(\tau)}{2U} + \frac{i\bar{\mu}\dot{\phi}_l(\tau)}{U} \right] \right\}. \qquad (10)$$

In Eq. (10) the effective coupling $J = tb_0^2$, while $\dot{\phi} = \partial_\tau \phi$ denotes the partial time derivative. As a consequence, the system of strongly interacting bosons has been transformed

into a system of weakly interacting bosonic particles (note that $J \sim t/U$) submerged in a fluctuating U(1) gauge field [32]. As a result, the linear response theory in Sec. II B is technically applied to a weakly interacting system; thus, its range of applicability is not violated. It is important to note that the phase variables $\phi_l(\tau)$ are defined up to an integer multiple of 2π; thus, the path integral in (9) must be performed with the boundary conditions $\phi_l(\beta) = \phi_l(0) + 2\pi \nu_l$, where $\nu_l = 0, \pm 1, \pm 2, \ldots$ are the winding numbers.

Next, we introduce the unitary fields $\zeta_l(\tau) = e^{i\phi_l(\tau)}$ and subsequently relax the constraint for the unit modulus of these fields to be fulfilled only on average, thus introducing a Lagrange multiplier λ [32,42]. This procedure allows us to obtain the analytic formula for the partition function in the form of a Gaussian integral:

$$Z = \int d\lambda \, e^{N\beta\lambda} \prod_{\mathbf{k},m} (d\bar{\zeta}_{\mathbf{k},m} d\zeta_{\mathbf{k},m}) \exp\left(-\frac{1}{N\beta} \bar{\zeta}_{\mathbf{k},m} \Gamma_{\mathbf{k},m}^{-1} \zeta_{\mathbf{k},m} \right), \qquad (11)$$

where we have performed the Fourier transform to the wave vector $\mathbf{k}$ and Matsubara frequency ω_m domain.

The propagator $\Gamma_{\mathbf{k},m}$ is defined as

$$\Gamma_{\mathbf{k},m}^{-1} \equiv \Gamma^{-1}(\mathbf{k}, \omega_m) = \lambda + \gamma_m^{-1} + J\varepsilon(\mathbf{k}), \qquad (12)$$

where $\varepsilon(\mathbf{k})$ is the dispersion of the lattice and $\gamma_m \equiv \gamma(\omega_m)$ is the Fourier transform of the single-site phase-phase correlator $\gamma(\tau - \tau') = \langle e^{i\phi_l(\tau) - i\phi_l(\tau')} \rangle$. In the low-temperature limit $\beta \to \infty$ the correlator can be written as

$$\gamma_m^{-1} = \frac{U}{4} \left\{ 1 - 4\left[v\left(\frac{\mu}{U}\right) + \frac{i\omega_m}{U} \right]^2 \right\}. \qquad (13)$$

The function $v(x) = x - \lfloor x \rfloor - 1/2$, where $\lfloor x \rfloor$ denotes the floor function, which gives the greatest integer less than or equal to x. The periodicity of $v(x)$ is a direct consequence of the periodicity of the phase variables on each lattice site.

The spatial correlation function $\langle \bar{a}_{\mathbf{k},m} a_{\mathbf{k},m} \rangle$ in Eq. (5), crucial to determine the transport properties of the system, can be calculated from the partition function (11):

$$\langle \bar{a}_{\mathbf{k},m} a_{\mathbf{k},m} \rangle = b_0^2 \langle \bar{\zeta}_{\mathbf{k},m} \zeta_{\mathbf{k},m} \rangle = N\beta \, b_0^2 \, \Gamma_{\mathbf{k},m}. \qquad (14)$$

The equation of state for our system reads

$$1 - \psi^2 = \frac{1}{N\beta} \sum_{\mathbf{k},m} \Gamma_{\mathbf{k},m}(\lambda = \lambda_0), \qquad (15)$$

where $\psi^2 = \langle e^{-i\phi_l(\tau)} \rangle^2$ denotes the phase order parameter [see Eq. (7)]. The Lagrange multiplier λ takes the stationary point value λ_0, which at the critical line and in the SF phase equals

$$\lambda_0^{SF} = \lambda_0^c = -J\varepsilon_0 - \gamma_0^{-1}, \qquad (16)$$

while in the MI phase $\lambda_0^{MI} = \lambda_0^{SF} + \delta\lambda$. The correction $\delta\lambda$ needs to be determined directly from Eq. (15).

Performing the summation over the Matsubara frequencies in Eq. (15) yields the equation of state in the following form:

$$1 - \psi^2 = \frac{1}{N} \sum_{\mathbf{k}} \frac{f_{\mathbf{k}}^+ + f_{\mathbf{k}}^-}{4\Xi_{\mathbf{k}}}, \qquad (17)$$

where the function

$$\frac{1}{\Xi_{\mathbf{k}}} = \left[\frac{J}{U}[\varepsilon(\mathbf{k}) - \varepsilon_0] + \frac{\delta\lambda}{U} + v^2\left(\frac{\mu}{U}\right) \right]^{-1/2} \quad (18)$$

can be interpreted as the ground-state distribution of the interacting bosons over the single-particle states and the functions

$$f_{\mathbf{k}}^{\pm} \equiv f_{\pm}(\beta, \Xi_{\mathbf{k}}) = \coth\left(\frac{\beta U}{2}\left[\Xi_{\mathbf{k}} \pm v\left(\frac{\mu}{U}\right) \right] \right) \quad (19)$$

are the thermal distributions of the excitations, with $+$ for the holelike excitations and $-$ for the particlelike excitations.

III. MOMENTUM-RESOLVED CONDUCTIVITY

We can now turn our attention to the derivation of the momentum-resolved conductivity. Substituting the explicit form of the spatial correlation function (14) into the Kubo linear formula for conductivity (4) yields

$$\sigma_{xx}(\mathbf{k}, \omega_v) = \frac{1}{N\omega_v} \frac{\pi^2 J^2}{\Phi_0^2 U} \sum_{\mathbf{q}} \left\{ [\sin(q_x) + \sin(q_x + k_x)]^2 F + [\sin^2(q_x) + \sin(q_x)\sin(q_x + k_x)]\left[\frac{f_{\mathbf{q}}^+ + f_{\mathbf{q}}^-}{\Xi_{\mathbf{q}}^3} + \frac{\beta U}{2}\frac{g_{\mathbf{q}}^+ + g_{\mathbf{q}}^-}{\Xi_{\mathbf{q}}^2} \right] \right\}, \quad (20)$$

where $g_{\mathbf{q}}^{\pm} \equiv g_{\pm}(\mathbf{q}) = \operatorname{csch}^2[\frac{\beta U}{2}(\Xi_{\mathbf{q}} \pm v)]$ and the function F is defined as

$$F = \frac{1}{\Xi_{\mathbf{q}}}\left[\frac{f_{\mathbf{q}}^-}{\left(\Xi_{\mathbf{q}} + \frac{i\omega_v}{U}\right)^2 - \Xi_{\mathbf{q}+\mathbf{k}}^2} + \frac{f_{\mathbf{q}}^+}{\left(\Xi_{\mathbf{q}} - \frac{i\omega_v}{U}\right)^2 - \Xi_{\mathbf{q}+\mathbf{k}}^2} \right] + \frac{1}{\Xi_{\mathbf{q}+\mathbf{k}}}\left[\frac{f_{\mathbf{q}+\mathbf{k}}^-}{\left(\Xi_{\mathbf{q}+\mathbf{k}} - \frac{i\omega_v}{U}\right)^2 - \Xi_{\mathbf{q}}^2} + \frac{f_{\mathbf{q}+\mathbf{k}}^+}{\left(\Xi_{\mathbf{q}+\mathbf{k}} + \frac{i\omega_v}{U}\right)^2 - \Xi_{\mathbf{q}}^2} \right]. \quad (21)$$

Next, we perform the analytic continuation to the real frequency domain, $\omega_v = \epsilon - i\omega$, where $\epsilon \to 0^+$. We will focus on the real part of the conductivity, where two types of terms can be distinguished, singular and regular:

$$\operatorname{Re}\sigma_{xx}(\mathbf{k}, \omega) = \operatorname{Re}\sigma_{xx}^{\text{sing}}(\mathbf{k}, \omega) + \operatorname{Re}\sigma_{xx}^{\text{reg}}(\mathbf{k}, \omega). \quad (22)$$

The singular part takes the form:

$$\operatorname{Re}\sigma_{xx}^{\text{sing}}(\mathbf{k}, \omega) = \frac{\pi^3 J^2}{N\Phi_0^2 U}\delta(\omega) \sum_{\mathbf{q}} \left\{ [\sin(q_x) + \sin(q_x + k_x)]^2 \frac{g_{\mathbf{q}+\mathbf{k}}^-(f_{\mathbf{q}+\mathbf{k}}^+ - h_{\mathbf{q}+\mathbf{k}}) - g_{\mathbf{q}}^-(f_{\mathbf{q}}^+ - h_{\mathbf{q}})}{2\Xi_{\mathbf{q}}(\Xi_{\mathbf{q}}^2 - \Xi_{\mathbf{q}+\mathbf{k}}^2)} \right. $$
$$\left. + [\sin^2(q_x) + \sin(q_x)\sin(q_x + k_x)]\left[\frac{f_{\mathbf{q}}^+ + f_{\mathbf{q}}^-}{\Xi_{\mathbf{q}}^3} + \frac{\beta U}{2}\frac{g_{\mathbf{q}}^+ + g_{\mathbf{q}}^-}{\Xi_{\mathbf{q}}^2} \right] \right\}, \quad (23)$$

with $h_{\mathbf{q}} = \cosh[\frac{\beta U}{2}(v - 3\Xi_{\mathbf{q}})]\operatorname{csch}[\frac{\beta U}{2}(\Xi_{\mathbf{q}} + v)]$, while the regular part is given as

$$\operatorname{Re}\sigma_{xx}^{\text{reg}}(\mathbf{k}, \omega) = \frac{\pi^3 J^2}{N\Phi_0^2 U} \sum_{\mathbf{q}} \frac{[\sin(q_x) + \sin(q_x + k_x)]^2}{2\Xi_{\mathbf{q}}\Xi_{\mathbf{q}+\mathbf{k}}}\left[\frac{f_{\mathbf{q}+\mathbf{k}}^- - f_{\mathbf{q}}^-}{\Xi_{\mathbf{q}} - \Xi_{\mathbf{q}+\mathbf{k}}}\delta(\omega + U[\Xi_{\mathbf{q}} - \Xi_{\mathbf{q}+\mathbf{k}}]) \right. $$
$$+ \frac{f_{\mathbf{q}+\mathbf{k}}^+ - f_{\mathbf{q}}^+}{\Xi_{\mathbf{q}} - \Xi_{\mathbf{q}+\mathbf{k}}}\delta(\omega - U[\Xi_{\mathbf{q}} - \Xi_{\mathbf{q}+\mathbf{k}}]) + \frac{f_{\mathbf{q}+\mathbf{k}}^+ + f_{\mathbf{q}}^-}{\Xi_{\mathbf{q}} + \Xi_{\mathbf{q}+\mathbf{k}}}\delta(\omega + U[\Xi_{\mathbf{q}} + \Xi_{\mathbf{q}+\mathbf{k}}])$$
$$\left. + \frac{f_{\mathbf{q}+\mathbf{k}}^- + f_{\mathbf{q}}^+}{\Xi_{\mathbf{q}} + \Xi_{\mathbf{q}+\mathbf{k}}}\delta(\omega - U[\Xi_{\mathbf{q}} + \Xi_{\mathbf{q}+\mathbf{k}}]) \right]. \quad (24)$$

The singular part of the conductivity involves the ballistic transport of thermal excitations with momentum $\mathbf{k}$. Due to the nondissipative nature of the system this behavior is present even in the disordered phase at nonzero temperature [19]. Additionally, the singular part contains the superfluid response, which is proportional to the order parameter Ψ_{SF} [19,31]. The regular part gives us insight into the possible types of excitations in the system. We will elaborate on that in the following sections.

A. Zero temperature

At zero temperature the formula for the regular part of the conductivity can be significantly simplified, as the first two terms in Eq. (24) vanish due to the vanishing difference of the thermal distributions $f_{\mathbf{q}}^{\pm}$.

As the conductivity is symmetric with respect to $\omega = 0$, we can restrict our analysis to only positive frequencies ω and further simplify formula (24):

$$\operatorname{Re}\sigma_{xx}^{\text{reg}}(\mathbf{k}, \omega) = \frac{\pi^3 J^2}{2N\Phi_0^2 U} \sum_{\mathbf{q}} [\sin(q_x) + \sin(q_x + k_x)]^2 $$
$$\times \frac{f_{\mathbf{q}+\mathbf{k}}^- + f_{\mathbf{q}}^+}{\Xi_{\mathbf{q}}\Xi_{\mathbf{q}+\mathbf{k}}(\Xi_{\mathbf{q}} + \Xi_{\mathbf{q}+\mathbf{k}})}$$
$$\times \delta(\omega - U[\Xi_{\mathbf{q}} + \Xi_{\mathbf{q}+\mathbf{k}}]). \quad (25)$$

The contribution to the regular part of the conductivity comes from the generation of a particle-hole pair with energy ω and momentum $\mathbf{k}$.
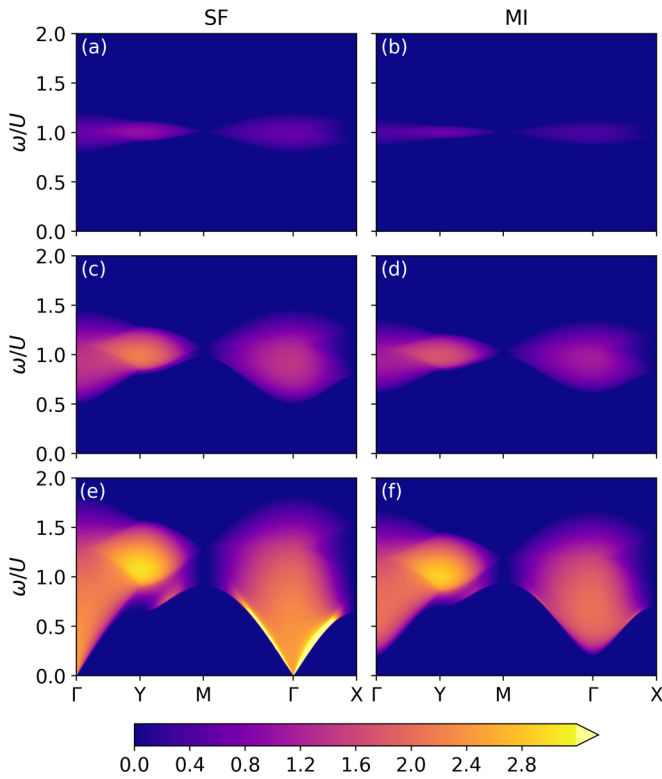
FIG. 1. Momentum-resolved conductivity for the square (2D) lattice at $T = 0$. Each row corresponds to one of three values of the chemical potential, (a) and (b) $\mu/U = 0.1$, (c) and (d) $\mu/U = 0.25$, and (e) and (f) $\mu/U = 0.5$. The hopping integral t/U was chosen to be at a fixed distance $\Delta(t/U)$ from the critical line. In the SF phase $\Delta(t/U) = 0.001$, (a) $t/U = 0.0341$, (c) $t/U = 0.0595$, and (e) $t/U = 0.0787$. In the MI phase $\Delta(t/U) = 0.01$, (b) $t/U = 0.0231$, (d) $t/U = 0.0485$, and (f) $t/U = 0.0677$.

The dependence of the conductivity on the frequency and momentum for 2D and 3D lattices is presented in Figs. 1 and 2, respectively.

The conductivity profile corresponds to the excitation spectra of the system. This is particularly evident in the different behaviors of conductivity in the superfluid and Mott insulator phases. In the MI phase, the conductivity channel becomes narrower, and the energy gap increases as a consequence of the smaller ratio of the hopping integral and repulsive energy t/U. Moreover, the conductivity values are smaller than in the SF phase because fewer particle-hole pairs can be created.

For small values of the chemical potential, $\mu/U = 0.1$ [as in Figs. 1(a), 1(b), 2(a), and 2(b)], the energy gap becomes more uniform in the momentum space as a consequence of the flattening of the energy bands (see Fig. 3).

On the other hand, for half-integer values of the chemical potential the lattice is uniformly filled with particles, and the energy gap closes at the Γ point of the first Brillouin zone, when the system is in the superfluid state [see Figs. 1(e) and 2(e)]. Moreover, the conductivity exhibits a linear dependence for small values of the momentum **k**. This results from the particle-hole symmetry present in the uniformly filled system. The lowest edge of the conductivity displays significantly different behaviors for the 2D and 3D lattices
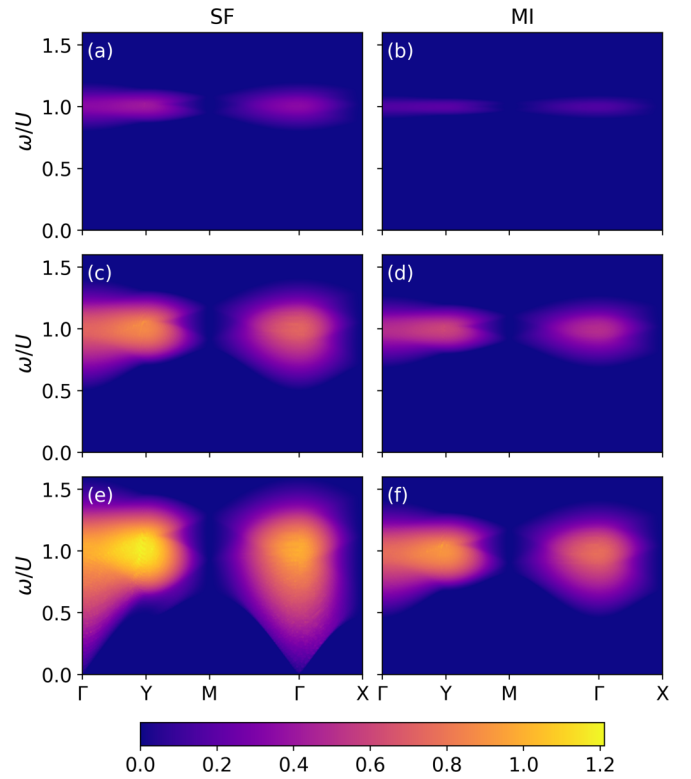

FIG. 2. Momentum-resolved conductivity for the cubic (3D) lattice at $T = 0$. The values of the chemical potential and hopping integral were chosen in the same manner as in Fig. 1. In the SF phase (a) $t/U = 0.0226$, (c) $t/U = 0.0364$, and (e) $t/U = 0.0415$. In the MI phase (b) $t/U = 0.0116$, (d) $t/U = 0.0264$, and (f) $t/U = 0.0315$.

(along the Γ-X and Γ-M lines). From Eq. (25) we can deduce that the integrand is singular at $\Xi_{\mathbf{q}+\mathbf{k}} = 0$ and is defined on a one-dimensional manifold for the 2D lattice. This leads to a logarithmic singularity at the edge of the spectrum. In contrast, for the 3D lattice, the integration is performed over a 2D manifold, which results in a finite jump at the edge of the spectrum, similar to the behavior of the 2D lattice density of states.

In the square lattice (the 2D system) at $\mu/U = 0.5$, the value of the conductivity at $\mathbf{k} = 0$, $\omega = 0$ becomes universal; that is, it does not depend on the microscopic parameters of the model [18–20,53,54]. This effect is not present in the MI
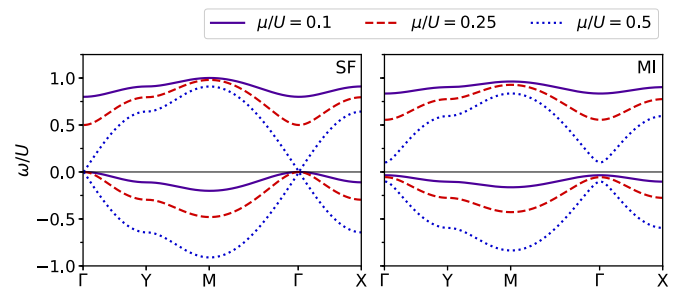

FIG. 3. Energy of the particle- and holelike excitations for the 2D lattice. The values of the hopping integrals correspond to the ones considered in Fig. 1.

phase. The energy gap remains open, and the conductivity exhibits quadratic dependence around $\mathbf{k} = 0$.

B. Group velocity

From the behavior of the momentum-resolved conductivity in a uniformly filled lattice, we can deduce the value of the group velocity of the excitations. Around the Γ point the energy gap behaves linearly with the momentum $\mathbf{k}$,

$$\frac{\omega_g}{U} = \alpha k_x, \tag{26}$$

where α is the slope of the line and the wave vector $\mathbf{k}$ was chosen to lie on the Γ-X line. The group velocity can be expressed in SI units as

$$v_g = \frac{U a}{2\hbar} \alpha. \tag{27}$$

We can estimate the value of the group velocity in a typical experiment. Taking as an example the celebrated experiment by Greiner *et al.* [55], in which ^{87}Rb atoms were placed in a 3D cubic optical lattice, we calculate the momentum-resolved conductivity for the system deep in the SF phase, $t/U \approx 0.227$. This corresponds to the potential depth $V_0 = 7E_r$, where E_r is the recoil energy. The slope α, determined from the conductivity map, is approximately 0.719, which yields a group velocity of the excitations of the order of $10^4 \, \mu$m/s.

There are experimental techniques which allow for extraction of the group velocity of the excitations from the atomic momentum distribution in ultracold bosonic systems [56]. Nevertheless, the rapid development of experimental methods of transport measurements [13] and momentum-resolved spectroscopy [57,58] could provide another way to determine the group velocity by studying the linear dependence of the energy gap of the conductivity in the long-wavelength limit.

C. Temperature effects

At nonzero temperature types of excitations other than just the creation of a particle-hole pair are available, i.e., the transition of a particle (or a hole) within the same band to a state with momentum shifted by $\mathbf{k}$ [see Eq. (24)]. A direct consequence of these new types of excitations is an additional channel of conductivity, which lies within the energy gap (see Figs. 4 and 5).

As the two-dimensional system (square lattice) exhibits only a zero-temperature phase transition, in agreement with Mermin-Wagner theorem [44], here we look at the three-dimensional (cubic) lattice because it allows us to observe the behavior of the conductivity in both ordered and disordered phases. In the normal phase (finite-temperature analog of the MI phase) the main conductivity channel shifts towards higher energies. This is a consequence of the additional phase deco-herence introduced by thermal fluctuations, which leads to the increase in the energy gap. In the SF phase we can observe a sharp line along the edge of the energy gap. This effect is most pronounced for $\mathbf{k}$ along the direction of the conductivity (we investigate the x component of the longitudinal conductivity σ_{xx}), while it vanishes for perpendicular $\mathbf{k}$, and it stems from
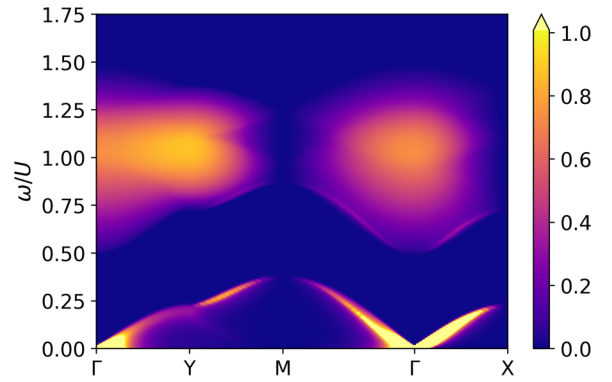

FIG. 4. Momentum-resolved conductivity for the 3D lattice at finite temperature $T/U = 0.04$ in the SF phase ($\mu/U = 0.25, t/U = 0.04$).

the fact that the external probe field acts only along the x direction.

IV. SUMMARY

In the present paper we have studied the momentum-resolved conductivity of strongly interacting bosons in the square (2D) and cubic (3D) lattices. The linear response theory combined with the quantum rotor approach to the Bose-Hubbard model allowed us to obtain the analytic formula for the conductivity. We have analyzed the behavior of the conductivity in both the superfluid and Mott insulator phases for chosen values of the chemical potential.

For the uniformly filled lattice the conductivity in the SF phase exhibits linear behavior in the vicinity of $\mathbf{k} = 0$, which is a direct consequence of the particle-hole symmetry present in the system. From the slope of the linear part we were able to estimate the group velocity of particle (or hole) excitations. We have also studied the influence of finite temperature on the current response and found that the thermal excitations lead to an additional channel in the conductivity spectrum.

The formalism presented in this paper can be applied to investigate the longitudinal and transverse conductivity in other types of lattices, including in the presence of artificial gauge fields. Growing interest in the physics of ultracold atomic
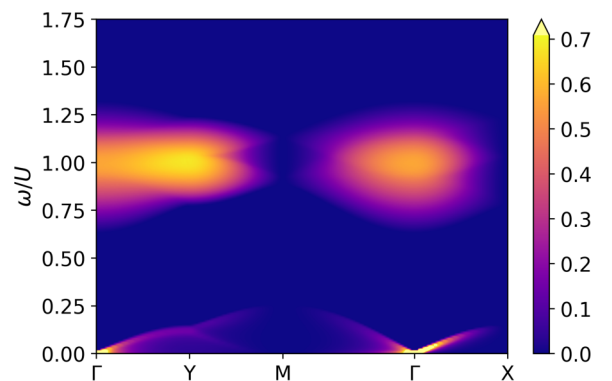

FIG. 5. Momentum-resolved conductivity for the 3D lattice at finite temperature $T/U = 0.04$ in the normal phase ($\mu/U = 0.25, t/U = 0.03$).

systems and rapid development of measurement techniques for transport properties [13] and correlation functions [57,58] could make it possible to verify the results presented in this work.

APPENDIX: GENERAL FORMULA FOR MOMENTUM-RESOLVED CONDUCTIVITY

In the following we present derivation of the general formula for the momentum-resolved conductivity in the Bose-Hubbard system. Starting with the formula for the conductivity in the linear response regime (4), we first perform the functional derivatives of the BH model partition function (2) over the vector potential $\mathbf{A}(\mathbf{r}, \tau)$. This yields

$$
\sigma_{xx}(\mathbf{k}, \omega_\nu) = -\frac{1}{N\beta\omega_\nu} \sum_{l,l'} \int_0^\beta d\tau \, d\tau' \, e^{i[\mathbf{k}(\mathbf{r}_l - \mathbf{r}_{l'}) - \omega_\nu(\tau - \tau')]}
$$

$$
\times \frac{\pi^2 t^2}{\Phi_0^2} \Big(\big\{ \big[\langle \bar{a}_{l'+e_x}(\tau') a_{l'}(\tau') \rangle + \langle \bar{a}_{l'}(\tau') a_{l'-e_x}(\tau') \rangle \big] - \text{c.c.} \big\} \big\{ \big[\langle \bar{a}_{l+e_x}(\tau) a_l(\tau) \rangle + \langle \bar{a}_l(\tau) a_{l-e_x}(\tau) \rangle \big] - \text{c.c.} \big\}
$$

$$
+ \big\langle \big\{ \big[\bar{a}_{l'+e_x}(\tau') a_{l'}(\tau') + \bar{a}_{l'}(\tau') a_{l'-e_x}(\tau') \big] - \text{c.c.} \big\} \big\{ \big[\bar{a}_{l+e_x}(\tau) a_l(\tau) + \bar{a}_l(\tau) a_{l-e_x}(\tau) \big] - \text{c.c.} \big\} \big\rangle \Big)
$$

$$
+ \frac{1}{N\beta\omega_\nu} \sum_{l,l'} \int_0^\beta d\tau \, d\tau' \, e^{i[\mathbf{k}(\mathbf{r}_l - \mathbf{r}_{l'}) - \omega_\nu(\tau - \tau')]}
$$

$$
\times \frac{\pi^2 t}{\Phi_0^2} \delta(\tau - \tau') \big\{ \big[\langle \bar{a}_{l+e_x}(\tau) a_l(\tau) \rangle + \text{c.c.} \big] (\delta_{l',l} + \delta_{l',l+e_x}) + \big[\langle \bar{a}_{l-e_x}(\tau) a_l(\tau) \rangle + \text{c.c.} \big] (\delta_{l',l} + \delta_{l',l-e_x}) \big\}, \tag{A1}
$$

where e_x denotes the unit vector in the x direction and the index $l + e_x = (l_x + 1, l_y, l_z)$ denotes the site neighboring site l.

Next, we perform the Fourier transform to the Matsubara frequency and momentum domains with the assumption that the system is defined on a square or cubic lattice:

$$
\sigma_{xx}(\mathbf{k}, \omega_\nu) = \frac{1}{(N\beta)^3 \omega_\nu} \frac{4\pi^2 t^2}{\Phi_0^2} \sum_{\mathbf{q}, \mathbf{q}'} \sum_{m, m'} [\sin(q_x) + \sin(q_x + k_x)][\sin(q_x') + \sin(q_x' + k_x)]
$$

$$
\times [\langle \bar{a}_{\mathbf{q}+\mathbf{k}, m+\nu} a_{\mathbf{q}, m} \rangle \langle \bar{a}_{\mathbf{q}', m} a_{\mathbf{q}'+\mathbf{k}, m+\nu} \rangle - \langle \bar{a}_{\mathbf{q}+\mathbf{k}, m+\nu} a_{\mathbf{q}, m} \bar{a}_{\mathbf{q}', m} a_{\mathbf{q}'+\mathbf{k}, m+\nu} \rangle]
$$

$$
+ \frac{1}{(N\beta)^2 \omega_\nu} \frac{4\pi^2 t}{\Phi_0^2} \sum_{\mathbf{q}, m} [\cos(q_x) + \cos(q_x + k_x)] \langle \bar{a}_{\mathbf{q}, m} a_{\mathbf{q}, m} \rangle. \tag{A2}
$$

The application of Wick's theorem [59], as well as the fact that within the QRA the averages $\langle \hat{a}^\dagger \hat{a} \rangle$ are diagonal in momentum and Matsubara frequencies [see Eq. (14)], allows us to write the conductivity in a more concise form:

$$
\sigma_{xx}(\mathbf{k}, \omega_\nu) = \frac{1}{(N\beta)^3 \omega_\nu} \frac{4\pi^2 t^2}{\Phi_0^2} \sum_{\mathbf{q}, m} [\sin(q_x) + \sin(q_x + k_x)]^2 \langle \bar{a}_{\mathbf{q}+\mathbf{k}, m+\nu} a_{\mathbf{q}+\mathbf{k}, m+\nu} \rangle \langle \bar{a}_{\mathbf{q}, m} a_{\mathbf{q}, m} \rangle
$$

$$
+ \frac{1}{(N\beta)^3 \omega_\nu} \frac{8\pi^2 t}{\Phi_0^2} \sum_{\mathbf{q}, m} [\sin^2(q_x) + \sin(q_x) \sin(q_x + k_x)] \langle \bar{a}_{\mathbf{q}, m} a_{\mathbf{q}, m} \rangle^2. \tag{A3}
$$

[1] M. Lewenstein, A. Sanpera, V. Ahufinger, B. Damski, A. Sen(De), and U. Sen, Adv. Phys. **56**, 243 (2007).

[2] I. Bloch, J. Dalibard, and W. Zwerger, Rev. Mod. Phys. **80**, 885 (2008).

[3] I. Bloch, J. Dalibard, and S. Nascimbène, Nat. Phys. **8**, 267 (2012).

[4] C. Gross and I. Bloch, Science **357**, 995 (2017).

[5] A. Tokuno and T. Giamarchi, Phys. Rev. Lett. **106**, 205301 (2011).

[6] Z. Wu, E. Taylor, and E. Zaremba, Europhys. Lett. **110**, 26002 (2015).

[7] C.-C. Chien, S. Peotta, and M. D. Ventra, Nat. Phys. **11**, 998 (2015).

[8] J.-P. Brantut, J. Meineke, D. Stadler, S. Krinner, and T. Esslinger, Science **337**, 1069 (2012).

[9] S. Krinner, D. Stadler, D. Husmann, J.-P. Brantut, and T. Esslinger, Nature (London) **517**, 64 (2015).

[10] D. Stadler, S. Krinner, J. Meineke, J.-P. Brantut, and T. Esslinger, Nature (London) **491**, 736 (2012).

[11] S. Krinner, D. Stadler, J. Meineke, J.-P. Brantut, and T. Esslinger, Phys. Rev. Lett. **110**, 100601 (2013).

[12] J.-P. Brantut, C. Grenier, J. Meineke, D. Stadler, S. Krinner, C. Kollath, T. Esslinger, and A. Georges, Science **342**, 713 (2013).

[13] S. Krinner, T. Esslinger, and J.-P. Brantut, J. Phys.: Condens. Matter **29**, 343003 (2017).

[14] M. Lebrat, S. Häusler, P. Fabritius, D. Husmann, L. Corman, and T. Esslinger, Phys. Rev. Lett. **123**, 193605 (2019).

[15] S. Häusler, S. Nakajima, M. Lebrat, D. Husmann, S. Krinner, T. Esslinger, and J.-P. Brantut, Phys. Rev. Lett. **119**, 030403 (2017).

[16] S. Kessler and F. Marquardt, Phys. Rev. A **89**, 061601(R) (2014).

[17] R. Anderson, F. Wang, P. Xu, V. Venu, S. Trotzky, F. Chevy, and J. H. Thywissen, Phys. Rev. Lett. **122**, 153602 (2019).

[18] C. Bruder, R. Fazio, A. Kampf, A. v. Otterlo, and G. Schön, Phys. Scr. **T42**, 159 (1992).

[19] A. van Otterlo, K.-H. Wagenblast, R. Fazio, and G. Schön, Phys. Rev. B **48**, 3316 (1993).

[20] T. K. Kopeć and J. V. José, Phys. Rev. B **60**, 7473 (1999).

[21] I. S. Beloborodov, Y. V. Fominov, A. V. Lopatin, and V. M. Vinokur, Phys. Rev. B **74**, 014502 (2006).

[22] A. P. Kampf and G. T. Zimanyi, Phys. Rev. B **47**, 279 (1993).

[23] A. Ivanov, G. Kordas, A. Komnik, and S. Wimberger, Eur. Phys. J. B **86**, 345 (2013).

[24] G. Kordas, D. Witthaut, P. Buonsante, A. Vezzani, R. Burioni, A. I. Karanikas, and S. Wimberger, Eur. Phys. J.: Spec. Top. **224**, 2127 (2015).

[25] A. R. Kolovsky, Z. Denis, and S. Wimberger, Phys. Rev. A **98**, 043623 (2018).

[26] A. A. Bychek, P. S. Muraev, D. N. Maksimov, and A. R. Kolovsky, Phys. Rev. E **101**, 012208 (2020).

[27] A. S. Sajna, T. P. Polak, and R. Micnas, Phys. Rev. A **89**, 023631 (2014).

[28] A. S. Sajna and T. P. Polak, Phys. Rev. A **90**, 043603 (2014).

[29] A. S. Sajna, T. P. Polak, and R. Micnas, Acta Phys. Pol. A **127**, 448 (2015).

[30] A. S. Sajna, Ann. Phys. (NY) **406**, 257 (2019).

[31] B. Grygiel, K. Patucha, and T. A. Zaleski, Phys. Rev. B **96**, 094520 (2017).

[32] T. P. Polak and T. K. Kopeć, Phys. Rev. B **76**, 094503 (2007).

[33] K. Patucha, B. Grygiel, and T. A. Zaleski, Phys. Rev. B **97**, 214522 (2018).

[34] M. P. A. Fisher, P. B. Weichman, G. Grinstein, and D. S. Fisher, Phys. Rev. B **40**, 546 (1989).

[35] D. Jaksch, C. Bruder, J. I. Cirac, C. W. Gardiner, and P. Zoller, Phys. Rev. Lett. **81**, 3108 (1998).

[36] D. R. Hofstadter, Phys. Rev. B **14**, 2239 (1976).

[37] J. Dalibard, F. Gerbier, G. Juzeliūnas, and P. Öhberg, Rev. Mod. Phys. **83**, 1523 (2011).

[38] H. Kleinert, *Path Integrals in Quantum Mechanics, Statistics, Polymer Physics, and Financial Market*, 3rd ed. (World Scientific, Singapore, 2004).

[39] H. Bruus and K. Flensberg, *Many-Body Quantum Theory in Condensed Matter Physics*, Oxford Graduate Texts (Oxford University Press, Oxford, 2004).

[40] S. Florens and A. Georges, Phys. Rev. B **66**, 165111 (2002).

[41] D. Pesin and L. Balents, Nat. Phys. **6**, 376 (2010).

[42] T. K. Kopeć, Phys. Rev. B **70**, 054518 (2004).

[43] T. K. Kopeć, Phys. Rev. B **73**, 104505 (2006).

[44] N. D. Mermin and H. Wagner, Phys. Rev. Lett. **17**, 1133 (1966).

[45] S. Sachdev, *Quantum Phase Transitions* (Cambridge University Press, Cambridge, 2000).

[46] H. Chamati, E. S. Pisanova, and N. S. Tonchev, Phys. Rev. B **57**, 5798 (1998).

[47] T. A. Zaleski and T. K. Kopeć, Phys. Rev. B **62**, 9059 (2000).

[48] F. P. Mancini, P. Sodano, and A. Trombettoni, Phys. Rev. B **67**, 014518 (2003).

[49] J. Ye, S. Sachdev, and N. Read, Phys. Rev. Lett. **70**, 4011 (1993).

[50] T. A. Zaleski and T. K. Kopeć, Phys. Rev. A **84**, 053613 (2011).

[51] T. P. Polak and T. A. Zaleski, Phys. Rev. A **87**, 033614 (2013).

[52] B. Grygiel, K. Patucha, and T. A. Zaleski, Phys. Rev. A **93**, 053607 (2016).

[53] M. P. A. Fisher, G. Grinstein, and S. M. Girvin, Phys. Rev. Lett. **64**, 587 (1990).

[54] M.-C. Cha, M. P. A. Fisher, S. M. Girvin, M. Wallin, and A. P. Young, Phys. Rev. B **44**, 6883 (1991).

[55] M. Greiner, O. Mandel, T. Esslinger, T. W. Hänsch, and I. Bloch, Nature (London) **415**, 39 (2002).

[56] T.-H. Leung, M. N. Schwarz, S.-W. Chang, C. D. Brown, G. Unnikrishnan, and D. Stamper-Kurn, Phys. Rev. Lett. **125**, 133001 (2020).

[57] T.-L. Dao, I. Carusotto, and A. Georges, Phys. Rev. A **80**, 023627 (2009).

[58] J. T. Stewart, J. P. Gaebler, and D. S. Jin, Nature (London) **454**, 744 (2008).

[59] A. L. Fetter and J. D. Walecka, *Quantum Theory of Many-Particle Systems* (McGraw-Hill, San Francisco, 1971).